Published by Oxford University Press *Human Molecular Genetics, 2001, Vol. 10, No. 6* ***555–564***

ARTICLE

Biochemical, phenotypic and neurophysiological characterization of a genetic mouse model of RSH/Smith–Lemli–Opitz syndrome

Christopher A. Wassif[1], Pinjun Zhu[2], Lisa Kratz[3], Patrycja A. Krakowiak[1], Kevin P. Battaile[4], Forrest F. Weight[2], Alexander Grinberg[5], Robert D. Steiner[4], Ngozi A. Nwokoro[1], Richard I. Kelley[3], Randall R. Stewart[2] and Forbes D. Porter[1,+]

[1]Heritable Disorders Branch, National Institute of Child Health and Human Development, National Institutes of Health, Building 10, Room 9S241, 10 Center Drive, Bethesda, MD 20892-1830, USA, [2]Laboratory of Molecular and Cellular Neurobiology, National Institute on Alcohol Abuse and Alcoholism, National Institutes of Health, Bethesda, MD 20892, USA, [3]The Johns Hopkins University, Kennedy Krieger Institute, Baltimore, MD 21205, USA, [4]Departments of Pediatrics and Molecular and Medical Genetics, Child Development and Rehabilitation Center, Doernbecher Children's Hospital, Oregon Health Sciences University, Portland, OR 07201, USA and [5]Laboratory of Mammalian Genes and Development, National Institute of Child Health and Human Development, National Institutes of Health, Bethesda, MD 20892, USA

Received 21 November 2000; Revised and Accepted 15 January 2001

The RSH/Smith–Lemli–Opitz syndrome (RSH/SLOS) is a human autosomal recessive syndrome characterized by multiple malformations, a distinct behavioral phenotype with autistic features and mental retardation. RSH/SLOS is due to an inborn error of cholesterol biosynthesis caused by mutation of the 3β-hydroxysterol Δ^7-reductase gene. To further our understanding of the developmental and neurological processes that underlie the pathophysiology of this disorder, we have developed a mouse model of RSH/SLOS by disruption of the 3β-hydroxysterol Δ^7-reductase gene. Here we provide the biochemical, phenotypic and neurophysiological characterization of this genetic mouse model. As in human patients, the RSH/SLOS mouse has a marked reduction of serum and tissue cholesterol levels and a marked increase of serum and tissue 7-dehydrocholesterol levels. Phenotypic similarities between this mouse model and the human syndrome include intra-uterine growth retardation, variable craniofacial anomalies including cleft palate, poor feeding with an uncoordinated suck, hypotonia and decreased movement. Neurophysiological studies showed that although the response of frontal cortex neurons to the neurotransmitter γ-amino-n-butyric acid was normal, the response of these same neurons to glutamate was significantly impaired. This finding provides insight into potential mechanisms underlying the neurological dysfunction seen in this human mental retardation syndrome and suggests that this mouse model will allow the testing of potential therapeutic interventions.

INTRODUCTION

The RSH/Smith–Lemli–Opitz syndrome (RSH/SLOS; OMIM 270400) is an autosomal recessive malformation/mental retardation syndrome caused by an inborn error of cholesterol metabolism. RSH/SLOS was first described by Smith, Lemli and Opitz in 1964 (1) and has an estimated incidence of 1/10 000 to 1/60 000 in populations of northern and central European heritage (2). The RSH/SLOS phenotype is variable, but typically includes craniofacial malformations, limb anomalies, growth retardation, behavioral problems and mental retardation (3,4). The cause of RSH/SLOS syndrome remained unknown until 1993 when Irons *et al.* (5) found decreased cholesterol and increased 7-dehydrocholesterol (7-DHC) levels in two RSH/SLOS patients. Subsequent work showed that RSH/SLOS is an inborn error of cholesterol biosynthesis due to a deficiency of 3β-hydroxysterol Δ^7-reductase activity, which results in impaired conversion of 7-DHC to cholesterol (Fig. 1A) (6–9). In the central nervous system (CNS), the 3β-hydroxysterol Δ^7-reductase also functions to reduce 7-dehydrodesmosterol (7-DHD) in the biosynthesis of desmosterol (Fig. 1A). The gene encoding the human 3β-hydroxysterol Δ^7-reductase (*DHCR7*) was identified based on homology to the sterol Δ^7-reductase from *Arabidopsis thaliana* and was mapped to human chromosome 11q12–13 (10,11). To date, more than 70 different mutations of *DHCR7* have been identified in patients with RSH/SLOS (2,11–13).

[+]To whom correspondence should be addressed. Tel: +1 301 435 4432; Fax: +1 301 480 5791; Email: fdporter@helix.nih.gov

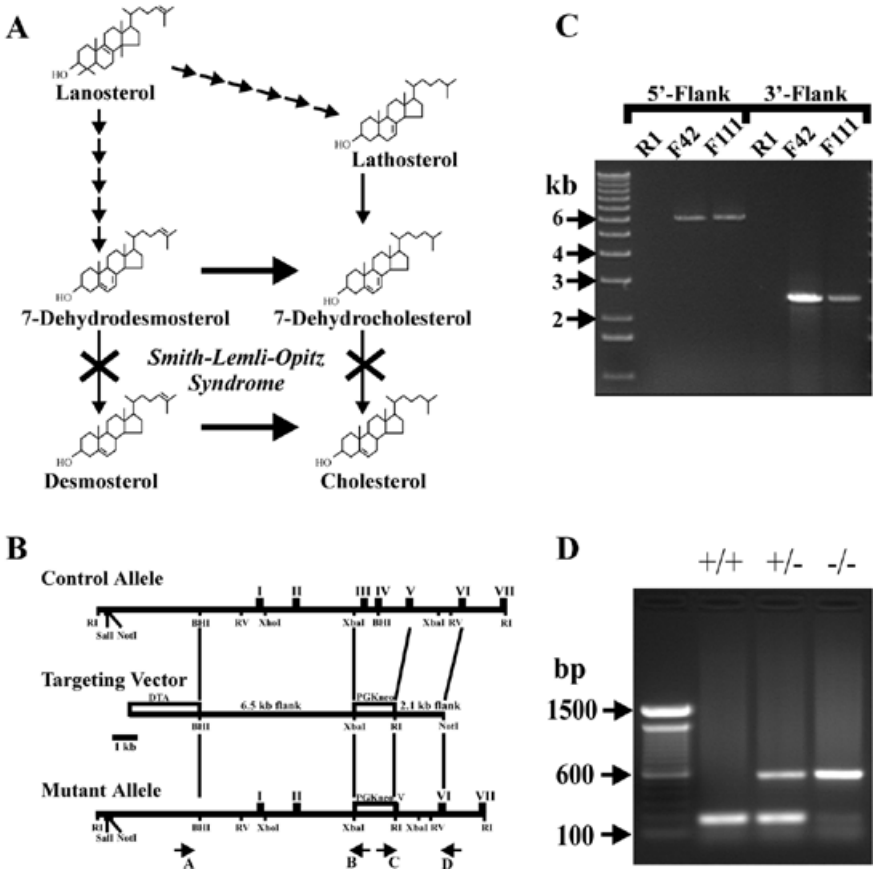

Figure 1. Targeted disruption of *Dhcr7*. (**A**) The reduction of both 7-DHD and 7-DHC to form desmosterol and cholesterol, respectively, is catalyzed by 3β-hydroxysterol Δ^7-reductase. These biosynthetic reactions are impaired in RSH/SLOS. (**B**) The *Dhcr7* genomic structure, targeting vector and resulting mutant allele. Filled boxes labeled with Roman numerals represent coding exons. RI, *Eco*RI; BHI, *Bam*HI; RV, *Eco*RV. Only relevant *Bam*HI sites are shown. The relative position of PCR primers used for identifying properly targeted ES cell clones are labeled A–D. (**C**) PCR analysis of untargeted R1 ES cells and two targeted ES cell clones (F42 and F111). Proper homologous recombination between the targeting vector and the wild-type allele was confirmed by PCR amplification of the 5′ and 3′ flanks using primer pairs A/B and C/D, respectively. (**D**) PCR genotyping of 1-day-old pups from a heterozygous *Dhcr7* intercross.

The functions of cholesterol during development and the biochemical mechanisms that underlie the dysmorphogenesis and neurological deficits seen in RSH/SLOS are only now being elucidated. Besides being a precursor for bile acids, neurosteroids and steroid hormones, cholesterol is a major lipid component of myelin and plasma membranes, it is necessary for the maturation of the hedgehog family of morphogens (14) and forms cholesterol rafts, which are involved in signal transduction (15). To further characterize the pathophysiology and neurophysiology underlying RSH/SLOS, and to provide a model system for testing therapeutic interventions, we produced a mouse model of RSH/SLOS by disruption of the mouse 3β-hydroxysterol Δ^7-reductase gene (*Dhcr7*). Similar to RSH/SLOS infants, *Dhcr7*$^{-/-}$ pups have variable craniofacial anomalies, demonstrate growth failure, are hypotonic and fail to feed.

RESULTS

Disruption of the *Dhcr7* gene

We disrupted the mouse 3β-hydroxysterol Δ^7-reductase gene (*Dhcr7*) in mouse embryonic stem (ES) cells using targeted homologous recombination (Fig. 1B). The replacement targeting vector was designed to disrupt *Dhcr7* by insertion of the neomycin phosphotransferase gene (*PGKneo*) and deletion of coding exons III, IV and part of exon V. Diphtheria toxin A subunit (DTA) was used to select against random insertional events. Cells that undergo non-homologous recombination with the targeting vector express DTA and are thus killed. Homologous recombination between the targeting vector and the *Dhcr7* allele was found in 12% (11/94) of G418-resistant ES cell clones. PCR amplification between primers located outside of the targeting flanks and internal to *PGKneo* were used to confirm proper homologous recombination by both the 5′ and 3′ flanks of the targeting vector with the *Dhcr7* allele in two independent G418-resistant clones (Fig. 1C). Southern blot analysis confirmed a single insertion of the targeting construct in both of these clones (data not shown). Both F42 and F111 clones produced germline transmitting chimeric founders. An identical phenotype was observed with both the F42 and F111 lines.

Heterozygous mice appeared phenotypically normal. Thus, we intercrossed *Dhcr7*$^{+/-}$ mice to determine if a recessive phenotype was present. Genotyping of 310 weaned progenies from heterozygous crosses identified no *Dhcr7*$^{-/-}$ animals

(38% +/+ and 62% +/–). In contrast, when all pups and embryos were genotyped (n = 587) we found a close to expected Mendelian ratio of 24% +/+, 50% +/– and 26% –/– (Fig. 1D). The *Dhcr7*$^{-/-}$ pups died during their first day of life, most likely as a consequence of their failure to feed.

Biochemical characterization of *Dhcr7*$^{-/-}$ mice

Biochemical characterization of sterol levels in tissues from *Dhcr7*$^{-/-}$ newborn pups showed that these mice had decreased cholesterol (Fig. 2A) and markedly increased 7-DHC levels (Fig. 2B) compared with either *Dhcr7*$^{+/+}$ or *Dhcr7*$^{+/-}$ pups. Serum 7-DHC levels in *Dhcr7*$^{-/-}$ pups were increased 1678-fold above serum levels measured in *Dhcr7*$^{+/+}$ pups. *Dhcr7*$^{-/-}$ tissue 7-DHC levels, compared with levels from *Dhcr7*$^{+/+}$ pups, were increased 250-, 265-, 250-, 791- and 2003-fold in cortex, midbrain, kidney, liver and muscle, respectively. Although minor compared to the increase seen in mutant pups, 7-DHC levels in *Dhcr7*$^{+/-}$ pups were elevated by 1.4–4.2-fold in tissues and by 9.6-fold in serum compared with levels in *Dhcr7*$^{+/+}$ pups. 8-Dehydrocholesterol (8-DHC), which is an isomer of 7-DHC (16), is also markedly elevated in mutant tissues (Fig. 2C). In the central nervous system, 3β-hydroxysterol Δ^7-reductase reduces 7-DHD to form desmosterol, and desmosterol levels were markedly reduced in cortex and midbrain from *Dhcr7*$^{-/-}$ pups compared with levels found in samples from either *Dhcr7*$^{+/+}$ or $^{+/-}$ pups (Fig. 2D). Consistent with a null mutation, 3β-hydroxysterol Δ^7-reductase activity in mutant fibroblasts, as measured by reduction of ergosterol to brassicasterol (17), was indistinguishable from background at 0.3% of control levels (Fig. 2E). Thin layer chromatography of ^{14}C-acetate-labeled steroids from *Dhcr7*$^{-/-}$ fibroblasts showed the same pattern of sterol intermediates as seen in human RSH/SLOS fibroblasts (data not shown). The accumulation of 7-DHC and 7-DHD during development of *Dhcr7*$^{-/-}$ embryos was characterized. In the livers of *Dhcr7*$^{-/-}$ embryos from embryonic day E12.5 until birth, 7-DHC accounts for ~50% of total sterols compared with very low levels in control embryos (Fig. 2F). Analysis of sterol content of brain tissue from *Dhcr7*$^{-/-}$ embryos showed that 7-DHC levels, as a percentage of total sterols, approach the level of cholesterol found in *Dhcr7*$^{+/+}$ embryos, whereas cholesterol levels decrease during development (Fig. 2G). In mutant embryos, 7-DHD levels progressively increased similar to the normal increase in desmosterol seen in *Dhcr*$^{+/+}$ embryos during development (Fig. 2H).

Phenotypic characterization of *Dhcr7*$^{-/-}$ pups

Homozygous mutant pups were growth retarded, had craniofacial malformations, demonstrated decreased movement and failed to feed (Fig. 3A and B). Failure to suckle is evident in that the mutant pups lack a milk spot (Fig. 3A). Intra-uterine growth retardation was observed (Fig. 3C) and mean birth weight for *Dhcr7*$^{-/-}$ pups was 1.11 ± 0.10 g (n = 68) compared with 1.44 ± 0.18 g (n = 46) for *Dhcr7*$^{+/+}$ pups ($P < 0.001$). Craniofacial anomalies were variably present in *Dhcr7*$^{-/-}$ pups. In 30% (20/67) of the *Dhcr7*$^{-/-}$ pups we noted the presence of a nasal plug and in 9% (6/67) of the animals we could not identify any nasal opening (Fig. 3D and E). The lack of a nasal opening was due to retention of a nasal plug in an otherwise normally formed nose (Fig. 3F–H). During development, a nasal plug is normally present from E16 until just prior to birth (18). The decreased movement and generalized weakness observed in the mutant pups may explain the lack of an expelled nasal plug. A cleft palate (Fig. 3I) was present in 9 of 111 *Dhcr7*$^{-/-}$ animals, compared with none in 115 control pups ($P < 0.01$, Fisher's exact test). Histological examination of the cleft palate found in *Dhcr7*$^{-/-}$ pups showed that the secondary palate had elevated, but failed to close to the midline (Fig. 3J and K). Histopathological analysis of heart, liver, spleen, pancreas, kidney, adrenal, spinal and trigeminal ganglia, vomeronasal structure, eye, small intestine, colon and myenteric plexus showed no significant abnormalities in *Dhcr7*$^{-/-}$ pups, whereas analysis of the lungs was notable for diffuse alveolar atelectasis (data not shown). No limb or skeletal malformations were detected by gross examination or examination of alizarin and alcian blue stained skeletal preparations (data not shown). Consistent with pups that have not fed, the bladder was dilated and meconium was present in the colon.

Neurophysiological characterization of *Dhcr7*$^{-/-}$ pups

The mutant pups lacked a milk spot, rarely vocalized alarm, had a hypotonic appearance and had less vigorous movements compared with controls (Fig. 3A and B). The decreased movement and hypotonic appearance were present at the time of birth and mutant pups were less vigorous than control pups that had not yet fed. Thus, these findings did not appear to be secondary to lack of feeding. The mutant pups were not rejected by the mother and the lack of feeding was observed in all *Dhcr7*$^{-/-}$ pups irrespective of craniofacial anomalies. Except for size, histopathological analysis by hematoxylin and eosin, trichrome, and phosphotungstic acid hematoxylin staining of skeletal muscle showed no significant differences between control and mutant animals (data not shown). Although smaller, mutant brain weights were proportional to body weight (controls, 5.2 ± 0.2% n = 8; mutants, 5.3 ± 0.1% n = 12), and TUNEL (TdT-mediated dUTP nick end-labeling) staining showed no increased apoptosis in brains of *Dhcr7*$^{-/-}$ pups (data not shown). A stereotypic rhythmic sucking/swallowing reflex was observed in control animals fed by hand. However, although the mutant pups could swallow formula, their swallowing movements lacked this rhythmic pattern. Hand feeding of *Dhcr7*$^{-/-}$ pups led to aspiration. When the mutant animals were fed dye-labeled formula, aspiration resulted in staining of the trachea, bronchi and lung parenchyma (Fig. 3M). This was not observed in control animals fed in a similar manner (Fig. 3L). Gross and histological examination of the pharynx and trachea revealed no malformations (data not shown).

The combination of decreased movement, uncoordinated suck/swallow and aspiration suggested a neurological defect which we postulated might be due to impairment of neuronal function by the replacement of 7-DHC and 7-DHD for cholesterol and desmosterol, respectively, in neuronal membranes. To test this hypothesis, whole-cell recordings were made from cortical neurons in brain slices. Neurons from both control and mutant pups exhibited similar reversible, tetrodotoxin-sensitive sodium currents in response to a voltage step to –30 mV from a holding potential of –90 mV (Fig. 4A and B). The mean peak amplitudes of the control (–828 ± 87 pA) and the mutant (–835 ± 81 pA) sodium currents were not significantly different (mean ± standard error, P = 0.9, unpaired t-test, n = 13 for both

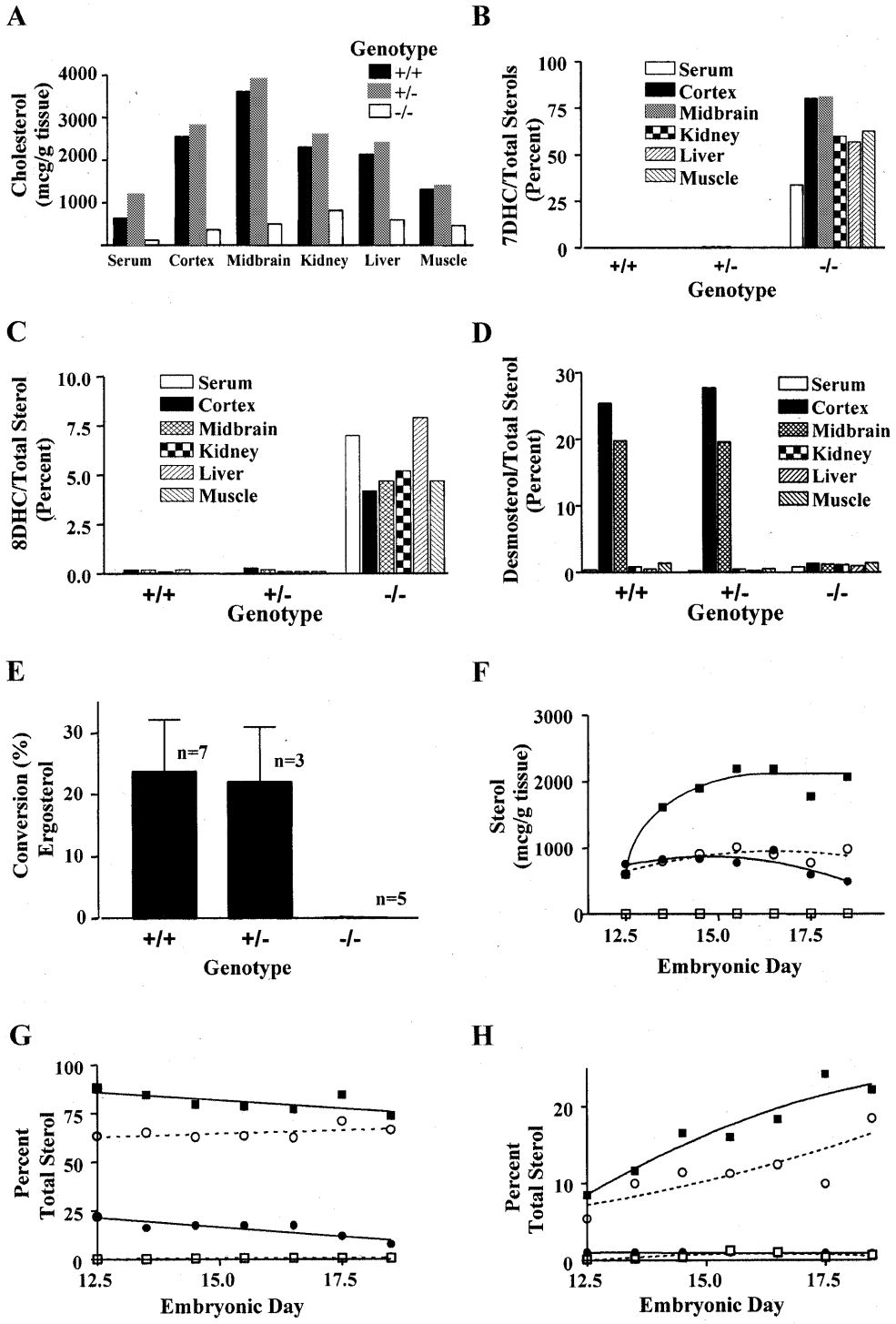

Figure 2. Biochemical analysis of *Dhcr7*$^{-/-}$ animals. Serum and tissue cholesterol (**A**) and 7-DHC (**B**) levels were measured by GC/MS in *Dhcr7*$^{+/+}$, $^{+/-}$ and $^{-/-}$ pups on the day of birth. Decreased cholesterol and increased 7-DHC levels were present in various tissues from *Dhcr7*$^{-/-}$ pups. (**C**) 8-Dehydrocholesterol levels were markedly increased in serum and tissue samples from *Dhcr7*$^{-/-}$ pups. (**D**) Desmosterol levels were markedly decreased in the cortex and midbrain of *Dhcr7*$^{-/-}$ pups compared with controls. (**E**) Reduction of ergosterol to brassicasterol was markedly reduced in skin fibroblasts from *Dhcr7*$^{-/-}$ animals ($P < 0.001$, unpaired *t*-test) compared with *Dhcr7*$^{+/+}$ skin fibroblasts. No significant difference was seen comparing fibroblasts derived from +/+ or +/– pups. (**F**) Liver cholesterol levels from +/+ (closed squares) and –/– (closed circles) embryos and 7-DHC levels from +/+ (open squares) and –/– (open circles) embryos determined by GC/MS during development. (**G**) Cholesterol (closed squares, +/+; closed circles, –/–) and 7-DHC (open squares, +/+; open circles, –/–) levels as a percentage of total sterols in the brains of developing embryos. (**H**) Desmosterol (closed squares, +/+; closed circles, –/–) and 7-DHD (open squares, +/+; open circles, –/–) levels as a percentage of total sterols in the brains of developing embryos. For the graphs (A–D) and (F–H), each data point represents the average of at least two determinations.

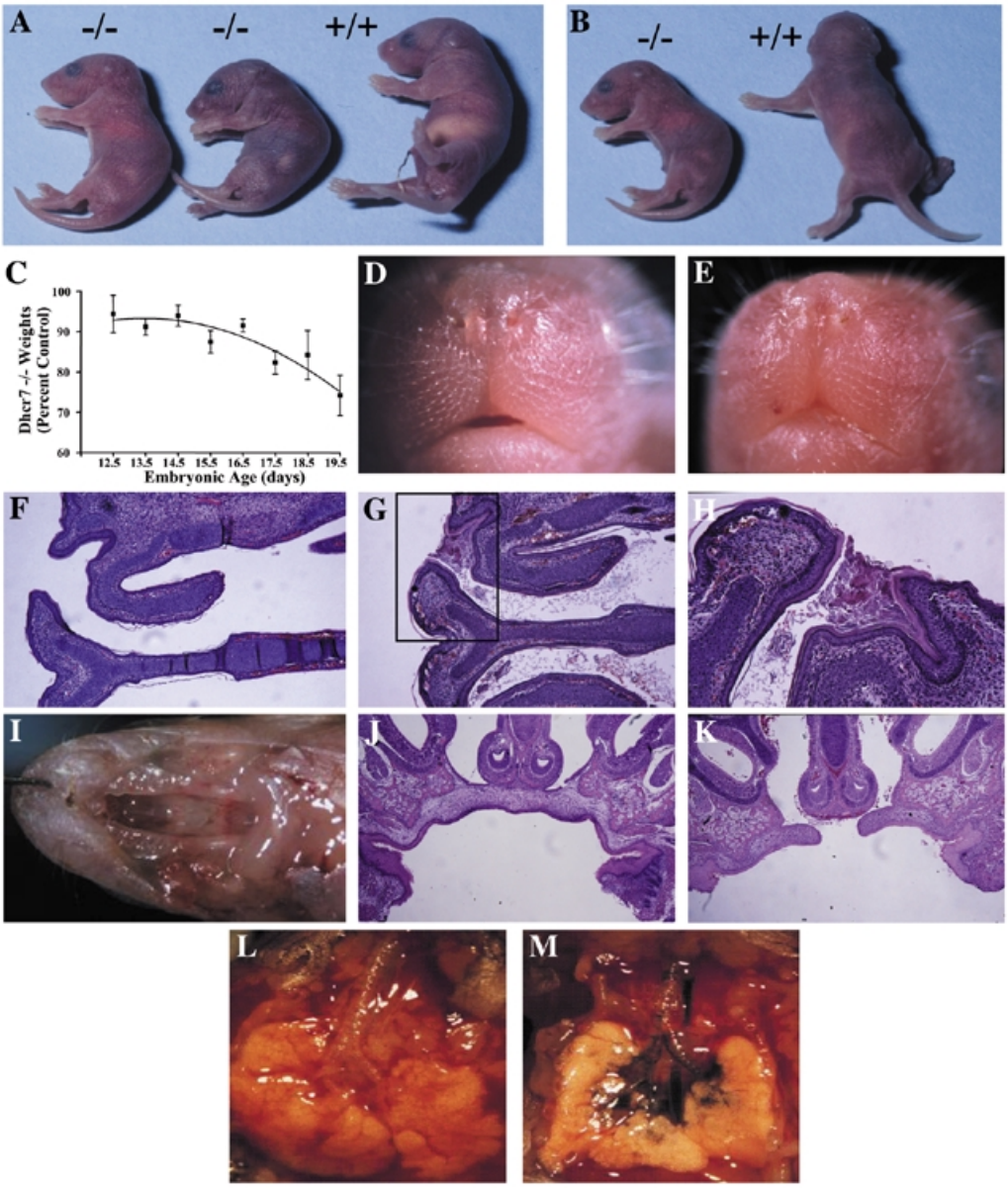

Figure 3. Phenotypic characterization of *Dhcr7*$^{-/-}$ mice. (**A**) *Dhcr7*$^{-/-}$ pups were smaller and lacked a milk spot. Some *Dhcr7*$^{-/-}$ pups lacked nasal openings and had cyanotic episodes (middle pup) consistent with obligate nasal breathing in newborn mice. (**B**) Decreased movement was characteristic of the *Dhcr7* mutant pups. (**C**) *Dhcr7*$^{-/-}$ pups demonstrated intra-uterine growth retardation which became more pronounced during the last 2 days of gestation. To account for litter size variability, the individual weights of the *Dhcr7*$^{-/-}$ embryos were normalized to the mean weight of the control embryos in that litter. Each data point represents the mean ± standard error for 3–14 mutant embryos from a minimum of two litters. (**D**) Prominent nasal openings are seen in this 1-day-old control pup. (**E**) The nasal openings are occluded in this newborn *Dhcr7*$^{-/-}$ pup. Hematoxylin- and eosin-stained transverse sectioning through the nasal region of a *Dhcr7*$^{+/+}$ (**F**) and *Dhcr7*$^{-/-}$ (**G**) newborn pup demonstrates the retention of a nasal plug in the mutant animals (10× magnification). (**H**) Higher magnification (20×) of the keratinized nasal plug found in many of the *Dhcr7*$^{-/-}$ animals. (**I**) Cleft palate was present in 9% of the *Dhcr7*$^{-/-}$ pups. Hematoxylin- and eosin-stained coronal sections comparing control *Dhcr7*$^{+/+}$ (**J**) and mutant *Dhcr7*$^{-/-}$ (**K**) pups demonstrated elevation of the palatal shelves but failure of the secondary palate to close in the midline. Hand-feeding of the mutant animals was precluded by aspiration. Eight microliters of dye-labeled infant formula were fed to control (**L**) and mutant (**M**) pups every 15 min for 6 h. Although the mutant animals were able to swallow the formula, dye labeling of the trachea, bronchi, and lungs was observed. The presence of dye-labeled formula in the esophagus of the mutant pup pictured was not a consistent finding and was observed in control pups. Although less intense labeling of the lungs was found in animals hand fed for shorter time periods, aspiration by the mutant pups was a consistent finding.

groups). Neurons from both control and mutant brains were able to generate a single action potential upon injection of a depolarizing current from a potential of –55 mV (data not shown). These control experiments establish that the mutant neurons are functionally similar to control neurons. We then tested the ability of mutant cortical neurons to respond to the neurotransmitters γ-amino-n-butyric acid (GABA) and glutamate. Although the median inward current was lower in mutant animals, no significant difference was seen in the response of control (Fig. 4C) and mutant (Fig. 4D) cortical neurons to 7.3 μM GABA. In control neurons the median amplitude of the inward current induced by GABA was –262 pA (–189 pA 25%

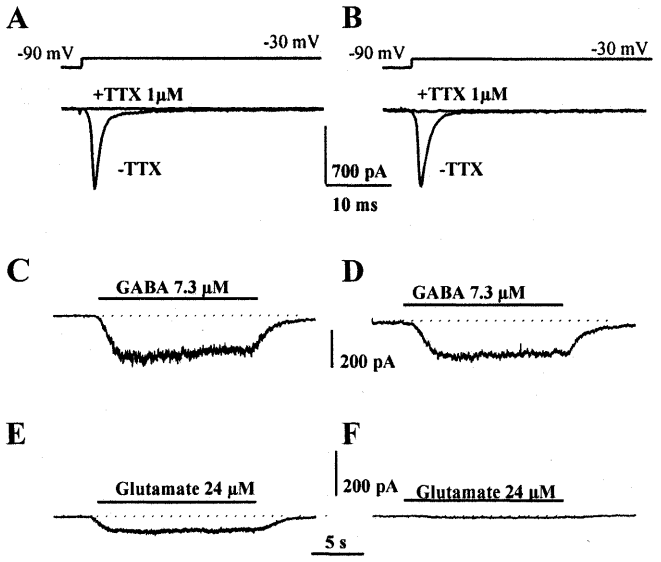

Figure 4. Neurophysiological characterization of *Dhcr7*$^{-/-}$ pups. Electrophysiological properties of newborn control and mutant neurons were recorded from the cerebral cortex in brain slices. Both control (**A**) and mutant (**B**) cortical neurons exhibited voltage-dependent inward sodium currents activated by a voltage step to –30 mV from a holding potential of –90 mV. The voltage step is shown above the current traces. Control (**C**) and mutant (**D**) cortical neurons showed a similar response to 7.3 μM GABA. Control cortical neurons (**E**) were significantly more sensitive to 24 μM glutamate than cortical neurons from *Dhcr7*$^{-/-}$ pups (**F**).

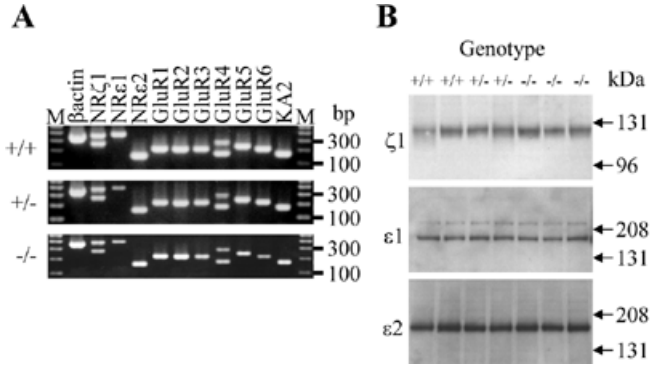

Figure 5. Expression of glutamate receptor subunits. (**A**) RT–PCR analysis demonstrates expression of the NMDAζ1, NMDAε1, NMDAε2, GluR1-4 (AMPA) and kainate (GluR5-6 and KA2) subunits in cerebral cortical total RNA from mutant and control animals. The two PCR products for GluR4 indicate transcripts coding for subunits with long and short C-termini. (**B**) Western blot analysis confirmed the presence of the NMDAζ1, NMDAε1 and NMDAε2 subunits in the cortex of mutant, heterozygous and homozygous wild-type pups. Densitometry measurements revealed no significant difference in expression of NMDAζ1 ($P = 0.37$), NMDAε1 ($P = 0.33$) and NMDAε2 ($P = 0.88$) between mutant ($n = 3$) and control ($n = 4$) animals (unpaired *t*-test).

and –514 pA 75%, $n = 13$) and the median amplitude for mutant cortical neurons was –161 pA (–88 pA 25% and –323 pA 75%, $n = 14$). These means were not statistically different ($P = 0.14$, Mann–Whitney rank sum test). In contrast, the neuronal response to the application of exogenous glutamate (24 μM), which stimulates NMDA (*N*-methyl-D-asparate), AMPA (α-amino-3-hydroxy-5-methyl-4-isoxazole propionic acid) and kainate glutamate receptors, was significantly reduced in mutant neurons (Fig. 4E and F). Application of glutamate induced a median inward current of –39 pA (–21 pA 25%, –67 pA 75%, $n = 14$) in control neurons, whereas *Dhcr7*$^{-/-}$ cortical neurons showed either a minimal response ($n = 9$) or no response ($n = 8$) to glutamate. In the 17 mutant cortical neurons from which glutamate responses were measured, the median current measured in response to glutamate was –4.9 pA (0 pA 25% and 11 pA 75%). Thus the median response to glutamate in mutant neurons was 12.5% of control level and the median mutant response was significantly different from the median control response ($P < 0.001$, Mann–Whitney rank sum test). The prolonged glutamate response recorded in control neurons is consistent with what is expected due to activation of NMDA glutamate receptors (19). One potential confounding factor is that a measured decrease in current induced by glutamate could be secondary to decreased cell surface area, which would result in decreased capacitance. However, if this result was due to a change in cell surface area, similar results would be expected for both the sodium current measurements and GABA-induced depolarization. The impaired glutamate response in *Dhcr7*$^{-/-}$ cortical neurons does not appear to be due to a developmental alteration of receptor expression. RT–PCR analysis established expression of NMDA, AMPA and kainate receptor subunits in mutant cortex (Fig. 5A) and western blot analysis detected no difference in cortical NMDAζ1, NMDAε1 or NMDAε2 subunit protein levels between mutants and controls (Fig. 5B).

DISCUSSION

RSH/SLOS is one of a few inborn errors of metabolism that present as a multiple malformation/mental retardation syndrome, and it is the prototypical example of a series of malformation syndromes now known to be due to inborn errors of post-squalene cholesterol biosynthesis. These other inborn errors of post-squalene cholesterol biosynthesis include desmosterolosis (20), X-linked dominant chondrodysplasia punctata of the Conradi–Hünermann type (21–23) and congenital hemidysplasia, ichthyosiform nevus and limb defects (CHILD) syndrome (24,25). Determination of the genetic and biochemical defects in this group of metabolic malformation syndromes has now provided the basis for understanding the biochemical, molecular, cellular and developmental processes that underlie the pathophysiology of these disorders. To further our mechanistic understanding of RSH/SLOS and to provide an experimental system in which therapeutic interventions could be tested, we produced a genetic mouse model of RSH/SLOS.

Our disruption of the *Dhcr7* gene was designed to produce a null mutation and we could not detect 3β-hydroxysterol Δ^7-reductase activity in skin fibroblasts from *Dhcr7*$^{-/-}$ pups using an ergosterol reduction assay. Characterization of sterols present in tissue and serum samples from *Dhcr7*$^{-/-}$ animals showed increased 7-DHC levels and decreased cholesterol levels compared to serum and tissue samples from control pups similar to that found in humans with RHS/SLOS. In addition to an accumulation of 7-DHC in the brains of *Dhcr7*$^{-/-}$ animals, we also found marked elevations of 7-DHD levels.

Dysmorphic features in this mouse model of RSH/SLOS were limited to retention of the nasal plug, intra-uterine growth retardation and cleft palate. Cleft palate was found in 9% of the

Dhcr7$^{-/-}$ pups. Cleft palate has been reported to be present in 37–47% of RSH/SLOS patients (3,4). No limb, renal, adrenal or CNS malformations were found. The relative lack of dysmorphic features, compared with what one expects to find in a human patient with two null mutations, may be due to placental transfer of maternal cholesterol during critical periods of development. Theoretically, the cholesterol ascertained in the *Dhcr7*$^{-/-}$ embryos could either be derived from maternal sources or synthesized *de novo* by an alternative biosynthetic pathway. In rodents, although most fetal cholesterol is derived by *de novo* synthesis (26), maternal cholesterol can cross the placenta and appears to be essential for early development (27). Placental transfer of maternal cholesterol to the developing fetus may explain the marked physical differences between our genetic mouse model and previously published teratogenic rodent models of RSH/SLOS. Fetuses from teratogenic rodent models using either AY9944 (28,29) or BM15.766 (30–32) to inhibit 3β-hydroxysterol Δ^7-reductase activity have major developmental malformations. The finding that maternal cholesterol supplementation partially ameliorates the teratogenic phenotype caused by AY9944 supports the idea that inhibition of maternal cholesterol biosynthesis is an etiological factor in these teratogenic model systems (28,29). A second possible explanation for the marked difference between these teratogenic models and our genetic model is that these teratogenic inhibitors lack specificity for the 3β-hydroxysterol Δ^7-reductase. In addition to inhibition of the 3β-hydroxysterol Δ^7-reductase, AY9944 has been reported to inhibit both the 3β-hydroxysterol Δ^{14}-reductase (33) and the 3β-hydroxysterol Δ^8-isomerase (34). In contrast to the major malformations induced by both AY9944 and BM15.766, teratogenic studies using YM9429 (35), another inhibitor of 3β-hydroxysterol Δ^7-reductase (36), report a cleft palate phenotype similar to that found in our genetic mouse model.

Squalene, which is synthesized via condensation of two molecules of farnesyl diphosphate, is the first cholesterol-specific intermediate of cholesterol biosynthesis. In addition to the *Dhcr7* mutant mouse, three additional post-squalene cholesterol biosynthesis mouse mutations have been described. These include disruption of squalene synthase, mutation of 3β-hydroxysteroid dehydrogenase (bare patches mouse) and mutation of sterol Δ^8–Δ^7 isomerase (tattered mouse). Disruption of the squalene synthase gene results in an autosomal recessive embryonic lethal phenotype. Many of the squalene synthase mutant embryos die prior to E9.5 and those that are recovered at E9.5 are developmentally retarded (37). Both the bare patches (Bpa) and tattered (Td) mutations are X-linked. Hemizygous Bpa males die shortly after implantation, whereas heterozygous females have hyperkeratotic skin lesions, asymmetric cataracts and chondrodysplasia (38). Male hemizygous Td embryos are growth retarded, edematous, have a cleft palate and craniofacial anomalies, lack intestines, have limb anomalies and die prenatally (23). Although a deficiency of any of these enzymes should inhibit endogenous cholesterol biosynthesis, the squalene synthase, Bpa, Td and *Dhcr7* mutant mice all have distinct phenotypes. This may be due to variable teratogenic effects of different precursor molecules or variable ability of the sterols that are synthesized to substitute for cholesterol.

Dhcr7$^{-/-}$ pups demonstrate marked neurological abnormalities. The neurological findings in the mutant pups, which include decreased movement and lack of suckling, are reminiscent of problems frequently encountered in RSH/SLOS infants. RSH/SLOS infants are frequently hypotonic and weak. Poor feeding and suck, which in many patients necessitates placement of a gastrostomy tube, is a frequently encountered clinical problem. The lack of a coordinated suck is consistent with an impaired response to glutamate during development. Pharmacological blockade of NMDA receptors in normal newborn mice impairs suckling (39) and disruption of the NMDAε2 (40) subunit results in uncoordinated suckling similar to that seen in *Dhcr7*$^{-/-}$ pups. Null mutations of the NMDAζ1 subunit (41,42) disturb both respiratory function and suckling (39) and a point mutation in the glycine binding site of the NMDAζ1 subunit results in pups that do not feed (43). Our neurophysiological investigations demonstrate that there is a decreased response of neurons from the frontal cortex of *Dhcr7*$^{-/-}$ mice to glutamate. This is a specific finding given that mutant neurons exhibit a normal sodium current, can generate normal action potentials and respond to GABA. In a recently published rat model of fetal alcohol syndrome, an elevated GABA response in conjunction with a decreased NMDA glutamate response was associated with increased neuronal apoptosis (44). This potential mechanism does not appear to be an etiological factor in our murine RSH/SLOS model. In mutant pups, brain weight was proportional to body weight, and no increased apoptosis was detected in brains from *Dhcr7*$^{-/-}$ pups. Both RT–PCR and western blot analysis established that the decreased glutamate response was not due to a developmental change in the expression of glutamate receptor subunits.

There are several possible explanations for the impaired glutamate response in *Dhcr7*$^{-/-}$ pups. The substitution of 7-DHD and 7-DHC for desmosterol and cholesterol in neuronal membranes could directly inhibit receptor function, inhibit subunit interactions or impair translocation of the receptor from the microsomal compartment to the synaptosomal membrane. Alternatively, decreased cholesterol levels or increased levels of cholesterol biosynthetic intermediates could indirectly modulate NMDA receptor function by affecting neurosteroid synthesis or function. Neurosteroids are thought to be endogenous ligands for sigma 1 (σ_1) receptors (45) and to modulate NMDA receptor function (46). Thus, decreased cholesterol levels could affect synthesis of neurosteroids. Additionally, the σ_1 receptor and enzymes of late cholesterol biosynthesis have significant structural and pharmacological similarities (47). Thus, elevations of sterol biosynthetic intermediates may competitively inhibit neurosteroid synthesis or affect neurosteroid interactions with σ_1 receptors.

We have established a genetic mouse model of RSH/SLOS. In addition to similar biochemical parameters, similarities between RSH/SLOS and this mouse model include cleft palate, growth retardation and neurological deficits. The impaired glutamate response observed in this mouse model may yield insight into the etiology of some of the neurological dysfunction seen in RSH/SLOS. Thus, this mouse model will be helpful in elucidating the biochemical and cellular basis of the neuropathophysiology underlying the behavioral and learning disabilities seen in this multiple malformation/mental retardation syndrome, and will also allow us to test potential therapeutic interventions.

MATERIALS AND METHODS

Construction of the *Dhcr7* targeting vector and mouse manipulation

Mouse expressed sequence tag 875323 was identified based on homology to the *A.thaliana* sterol Δ^7-reductase sequence. A genomic bacterial artificial chromosome (BAC) clone was isolated by PCR screening of a mouse 129 BAC library 5′-GCAGCCTTGGGAAGCATAGAGAGG-3′ and 5′-ACCAGGATGGCCCAATCATCGGAG-3′ (Genome Systems). To generate the targeting construct, a 6.5 kb *Bam*HI/*Xba*I 5′ flank fragment was cloned into pBS. The neomycin phosphotransferase gene was cloned into this construct as an *Xba*I/*Eco*RI fragment. The 3′-flank was generated as a 2.1 kb PCR fragment (5′-CCGGAATTCCCTCATTAACCTGTCCTTCGC-3′ and 5′-ATAAGAATGCGGCCGCCGATGGTCTTCAGATACCAGG-3′) and was cloned as an *Eco*RI/*Not*I fragment. The negative selectable marker, DTA, was cloned into a *Sal*I site. The targeting vector pAH-7 was linearized with *Not*I. The targeting construct was electroporated into J1 ES cells (Bio-Rad Electroporator, 400 V, 25 μF), which were then plated at a density of 5×10^5 cells into a 60 mm dish containing a layer of G418-resistant embryonic fibroblasts. Selection for G418 (350 mcg/ml; Gibco BRL) resistant colonies was begun 24 h after plating. Culture conditions and media were as previously described (48). Screening of G418-resistant clones was done by PCR using primers internal to the neomycin resistance gene and primers external to the targeting construct flank. To establish homologous recombination on the 5′ flank, primers A and B were used (A, 5′-CAGTGAGGCTCGGGAGTGGAAGG-3′; B, 5′-CAAATTAAGGGCCAGCTCATTCCTCC-3′). Homologous recombination of the 3′ flank was established using primers C and D (C, 5′-GAGGCCAGAGGCCACTTGTGAGCG-3′; D, 5′-GCCTAGGTACCACCCAAAGTGG-3′). Clones F42 and F111 were microinjected into C57/B6 blastocysts using standard techniques. Four PCR primers were used in a combined reaction to genotype the mice in this study. These were mutant 5′-CATCCCCTCAGAAGAACTCGT-3′, mutant 5′-CTGTGCTCGACGTTGTCACTG-3′, which produced a 600 bp fragment originating from the neomycin phosphotransferase gene, wild-type 5′-GGTGAATGGGCTGCZAAGCCTGG-3′ and wild-type 5′-GGTAGCCCTTGATCATTGCG-3′, which produced a 200 bp fragment originating from exon IV which is deleted in the mutant allele. PCR cycling conditions consisted of 5 min of denaturation at 94°C followed by 35 cycles of 30 s at 94°C, 60 s at 63°C, 60 s at 72°C and a final extension of 10 min at 72°C. For timed matings, the identification of a copulatory plug was considered to be E0.5 and embryonic age was confirmed by inspection. This animal work was done under NICHD and NIAAA approved animal study protocols.

Sterol, enzymatic, histological, RT–PCR and western blot analysis

Sterols were extracted from serum and tissues and analyzed by GC/MS as previously described (8). The rate of conversion of ergosterol to brassicasterol was measured as previously described (17). Standard histologic techniques and staining were used. For RT–PCR, total RNA was isolated from cerebral cortex of wild-type (n = 3), heterozygous (n = 1) and mutant (n = 2) mice, subjected to DNase I (Amplification grade, Life Technologies) to eliminate potential genomic DNA contamination, reverse transcribed with random hexamers and Moloney Murine Leukemia Virus reverse transcriptase (Life Technologies) and amplified by PCR for 40 cycles of 30 s at 92°C, 90 s at 55°C and 60 s at 72°C using the following primer sets: β-actin forward 5′-ACAGCTGAGAGGGAAATCGTG-3′ and reverse 5′-CTAGGAGCCAGGGCAGTAATCT-3′ (expected product 362), NMDARζ1 forward 5′-ATGCCCCTGCCACCCTCACTTTTG-3′ and reverse 5′-GCAGCTGGCCCTCCTCCCTCTCA-3′ (expected products 381 and 270 bp), NMDARε1 forward 5′-CGGGAGGGATGAAGGCTGTAA-3′ AC-3′ and reverse 5′-TGTAGATGCCCCTGCTGATGGAGA-3′ (390 bp), NMDARε2 5′-CTGCCGGACACCATCACAACAATC-3′ and reverse 5′-CACCGTGGGCTGCCTGAAGAAGTA-3′ (157 bp), GluR1 forward 5′-CAGCGGAGGAAGTGGCAGTG-3′ and reverse 5′-GAGGCGGTGTTTCATTTCTTTGTT-3′ (222 bp), GluR2 forward 5′-CAAGGCAAGGCTGTCAAT-3′ and reverse 5′-GATATCGGATGCCTCTCACC-3′ (219 bp), GluR3 forward 5′-AACTCACAAAGAACACCCAAAACT-3′ and reverse 5′-TCATGCCCGACACCAAGGAG-3′ (216 bp), GluR4 forward 5′-AGCAGGCGTCTTCTACATTC-3′ and reverse 5′-CACGGCCGTTTTCTCCCACACT-3′ (176 and 289 bp), GluR5 forward 5′-CACGACACATATTTGGAGGAC-3′ and reverse 5′-CCGCTTGTTTATTATTATTTAGAA-3′ (244 bp), GluR6 forward 5′-AAGAGGTTTTTAATGATGAGGTC-3′ and reverse 5′-CAGTTTGTGCTTGGGTGAT-3′ (215 bp) and KA2 forward 5′-GCGTGCGCCGACTGACT-3′ and reverse 5′-GCCACGGTGCGGATAGAAT-3′ (168 bp). PCR products were visualized on 2% agarose gels containing ethidium bromide. For western blot analysis, tissue extracts were made in RIPA buffer (1× PBS, 1% NP-40, 0.5% sodium deoxycholate, 0.1% SDS). Protein was determined using the Bio-Rad DC Protein Assay. Twenty-five micrograms of protein were separated on 7% NuPage Tris–acetate gels (Invitrogen) according to the manufacturer's protocol. Equivalent protein loading was confirmed by Coomassie Blue staining of a parallel gel. Proteins were then transferred to a nitrocellulose membrane and chemoluminescent western blotting was performed using the WesternBreeze kit by Invitrogen. Affinity purified goat polyclonal IgG primary antibodies from Santa Cruz Biotechnology [NMDAε1 (sc-1468), NMDAε2 (sc-1469) and NMDAε3 (sc-1470)] were used at a dilution of 1:100.

Whole-cell patch clamp of cerebral cortical neurons in brain slices

Horizontal brain slices (450–600 μm) were prepared within 24 h after birth. The composition of the external recording buffer (ACSF) was: 124 mM NaCl, 3 mM KCl, 2 mM $CaCl_2$, 1.3 mM $MgSO_4$, 1.2 mM Na_2HPO_4, 25 mM $NaCO_3$ and 10 mM glucose. The slice was continuously perfused (4 ml/min) with ACSF and oxygenated with a 95%/5% mixture of O_2/CO_2 at room temperature (23°C) in a recording chamber. Drugs were applied by gravity flow through a micropipette placed ~150 μm from the recording site. Frontal cerebral cortex neurons were visualized under an Axioskop 2FS fixed-stage microscope (Zeiss). Patch pipettes were made by a two-stage microelectrode puller (PC-10, Narishige) and filled with internal solution containing 140 mM CsCl, 10 mM HEPES, 5.5 mM BAPTA, 2.0 mM $MgCl_2$ and 2.0 mM Mg–ATP. Whole-cell

current was measured with conventional patch clamp techniques (Axopatch 200B, Axon Instruments). Holding potential was –60 mV. The data were acquired by pClamp8 software through a Digidata 1200 interface. Data were plotted with SigmaPlot. GABA, tetrodotoxin and glutamate were obtained from Sigma.

ACKNOWLEDGEMENTS

We would like to thank Sing-Ping Huang and Dr Heiner Westphal for their assistance with production of the *Dhcr7* mutant mice and Dr Diana Hanes (SAIC) and Dr Raj P. Kapur for their assistance with the histopathological analysis. R.D.S. was supported by the Oregon Child Health Research Center grant PHS 5P30-HD33703-04 from the NICHD and, as a clinical associate physician investigator from the NCRR, grant RR00334-33S3.

REFERENCES

1. Smith, D.W., Lemli, L. and Opitz, J.M. (1964) A newly recognized syndrome of multiple congenital anomalies. *J. Pediatr.*, **64**, 210–217.
2. Porter, F.D .(2000) RSH/Smith–Lemli–Opitz syndrome: a multiple congenital anomaly/mental retardation syndrome due to an inborn error of cholesterol biosynthesis. *Hum. Mol. Genet.*, **71**, 163–174.
3. Ryan, A.K., Bartlett, K., Clayton, P., Eaton, S., Mills, L., Donnai, D., Winter, R.M. and Burn, J. (1998) Smith-Lemli-Opitz syndrome: a variable clinical and biochemical phenotype. *J. Med. Genet.*, **35**, 558–565.
4. Kelley, R.I. and Hennekam, R.C. (2000) The Smith-Lemli-Opitz syndrome. *J. Med. Genet.*, **37**, 321–335.
5. Irons, M., Elias, E.R., Salen, G., Tint, G.S. and Batta, A.K. (1993) Defective cholesterol biosynthesis in Smith-Lemli-Opitz syndrome. *Lancet*, **341**, 1414.
6. Tint, G.S., Irons, M., Elias, E.R., Batta, A.K., Frieden, R., Chen, T.S. and Salen, G. (1994) Defective cholesterol biosynthesis associated with the Smith-Lemli-Opitz syndrome. *N. Engl. J. Med.*, **330**, 107–113.
7. Tint, G.S., Seller, M., Hughes-Benzie, R., Batta, A.K., Shefer, S., Genest, D., Irons, M., Elias, E. and Salen, G. (1995) Markedly increased tissue concentrations of 7-dehydrocholesterol combined with low levels of cholesterol are characteristic of the Smith-Lemli-Opitz syndrome. *J. Lipid Res.*, **36**, 89–95.
8. Kelley, R.I. (1995) Diagnosis of Smith-Lemli-Opitz syndrome by gas chromatography/mass spectrometry of 7-dehydrocholesterol in plasma, amniotic fluid and cultured skin fibroblasts. *Clin. Chim. Acta*, **236**, 45–58.
9. Shefer, S., Salen, G., Batta, A.K., Honda, A., Tint, G.S., Irons, M., Elias, E.R., Chen, T.C. and Holick, M.F. (1995) Markedly inhibited 7-dehydrocholesterol-delta 7-reductase activity in liver microsomes from Smith-Lemli-Opitz homozygotes. *J. Clin. Invest.*, **96**, 1779–1785.
10. Moebius, F.F., Fitzky, B.U., Lee, J.N., Paik, Y.-K. and Glossmann, H. (1998) Molecular cloning and expression of the human delta 7-sterol reductase. *Proc. Natl Acad. Sci. USA*, **95**, 1899–1902.
11. Wassif, C.A., Maslen, C., Kachilele-Linjewile, S., Lin, D., Linck, L.M., Connor, W.E., Steiner, R.D. and Porter, F.D. (1998) Mutations in the human sterol delta7-reductase gene at 11q12-13 cause Smith-Lemli-Opitz syndrome. *Am. J. Hum. Genet.*, **63**, 55–62.
12. Fitzky, B.U., Witsch-Baumgartner, M., Erdel, M., Lee, J.N., Paik, Y.K., Glossmann, H., Utermann, G. and Moebius, F.F. (1998) Mutations in the delta7-sterol reductase gene in patients with the Smith-Lemli-Opitz syndrome. *Proc. Natl Acad. Sci. USA*, **95**, 8181–8186.
13. Waterham, H.R., Wijburg, F.A., Hennekam, R.C., Vreken, P., Poll-The, B.T., Dorland, L., Duran, M., Jira, P.E., Smeitink, J.A., Wevers, R.A. and Wanders, R.J. (1998) Smith-Lemli-Opitz syndrome is caused by mutations in the 7-dehydrocholesterol reductase gene. *Am. J. Hum. Genet.*, **63**, 329–338.
14. Beachy, P.A., Cooper, M.K., Young, K.E., von Kessler, D.P., Park, W.J., Hall, T.M., Leahy, D.J. and Porter, J.A. (1997) Multiple roles of cholesterol in hedgehog protein biogenesis and signaling. *Cold Spring Harb. Symp. Quant. Biol.*, **62**, 191–204.
15. Simons, K. and Ikonen, E. (1997) Functional rafts in cell membranes. *Nature*, **387**, 569–572.
16. Batta, A.K., Tint, G.S., Shefer, S., Abuelo, D. and Salen, G. (1995) Identification of 8-dehydrocholesterol (cholesta-5,8-dien-3 beta-ol) in patients with Smith-Lemli-Opitz syndrome. *J. Lipid Res.*, **36**, 705–713.
17. Honda, M., Tint, G.S., Honda, A., Batta, A.K., Chen, T.S., Shefer, S. and Salen, G. (1996) Measurement of 3 beta-hydroxysteroid delta 7-reductase activity in cultured skin fibroblasts utilizing ergosterol as a substrate: a new method for the diagnosis of the Smith-Lemli-Opitz syndrome. *J. Lipid Res.*, **37**, 2433–2438.
18. Rugh, R. (1968) *The Mouse: Its Reproduction and Development.* Oxford University Press, New York, NY.
19. Dingledine, R., Borges, K., Bowie, D. and Traynelis, S.F. (1999) The glutamate receptor ion channels. *Pharmacol. Rev.*, **51**, 7–61.
20. FitzPatrick, D.R., Keeling, J.W., Evans, M.J., Kan, A.E., Bell, J.E., Porteous, M.E., Mills, K., Winter, R.M. and Clayton, P.T. (1998) Clinical phenotype of desmosterolosis. *Am. J. Med. Genet.*, **75**, 145–152.
21. Kelley, R.I., Wilcox, W.G., Smith, M., Kratz, L.E., Moser, A. and Rimoin, D.S. (1999) Abnormal sterol metabolism in patients with Conradi-Hunermann-Happle syndrome and sporadic lethal chondrodysplasia punctata. *Am. J. Med. Genet.*, **83**, 213–219.
22. Braverman, N., Lin, P., Moebius, F.F., Obie, C., Moser, A., Glossmann, H., Wilcox, W.R., Rimoin, D.L., Smith, M., Kratz, L. *et al.* (1999) Mutations in the gene encoding 3 beta-hydroxysteroid-delta 8, delta 7-isomerase cause X-linked dominant Conradi-Hunermann syndrome. *Nature Genet.*, **22**, 291–294.
23. Derry, J.M., Gormally, E., Means, G.D., Zhao, W., Meindl, A., Kelley, R.I., Boyd, Y. and Herman, G.E. (1999) Mutations in a delta 8-delta 7 sterol isomerase in the tattered mouse and X-linked dominant chondrodysplasia punctata. *Nature Genet.*, **22**, 286–290.
24. Grange, D.K., Kratz, L.E., Braverman, N.E. and Kelley, R.I. (2000) CHILD syndrome caused by deficiency of 3beta-hydroxysteroid-delta8, delta7-isomerase. *Am. J. Med. Genet.*, **90**, 328–335.
25. Konig, A., Happle, R., Bornholdt, D., Engel, H. and Grzeschik, K.H. (2000) Mutations in the NSDHL gene, encoding a 3beta-hydroxysteroid dehydrogenase, cause CHILD syndrome. *Am. J. Med. Genet.*, **90**, 339–346.
26. Jurevics, H.A., Kidwai, F.Z. and Morell, P. (1997) Sources of cholesterol during development of the rat fetus and fetal organs. *J. Lipid Res.*, **38**, 723–733.
27. Willnow, T.E., Hilpert, J., Armstrong, S.A., Rohlmann, A., Hammer, R.E., Burns, D.K. and Herz, J. (1996) Defective forebrain development in mice lacking gp330/megalin. *Proc. Natl Acad. Sci. USA*, **93**, 8460–8464.
28. Roux, C., Horvath, C. and Dupuis, R. (1979) Teratogenic action and embryo lethality of AY9944. Prevention by a hypercholesterolemia-provoking diet. *Teratology*, **19**, 35–38.
29. Barbu, V., Roux, C., Dupuis, R., Gardette, J. and Maziere, J. (1988) Cholesterol prevents the teratogenic action of AY9944: importance of the timing of cholesterol supplementation to rats. *J. Nutr.*, **118**, 774–779.
30. Kolf-Clauw, M., Chevy, F., Siliart, B., Wolf, C., Mulliez, N. and Roux, C. (1997) Cholesterol biosynthesis inhibited by BM15.766 induces holoprosencephaly in the rat. *Teratology*, **56**, 188–200.
31. Dehart, D.B., Lanoue, L., Tint, G.S. and Sulik, K.K. (1997) Pathogenesis of malformations in a rodent model for Smith-Lemli-Opitz syndrome. *Am. J. Med. Genet.*, **68**, 328–337.
32. Lanoue, L., Dehart, D.B., Hinsdale, M.E., Maeda, N., Tint, G.S. and Sulik, K.K. (1997) Limb, genital, CNS, and facial malformations result from gene/environment-induced cholesterol deficiency: further evidence for a link to sonic hedgehog. *Am. J. Med. Genet.*, **73**, 24–31.
33. Lutsky, B.N., Hsiung, H.M. and Schroepfer, G.J. (1975) Inhibition of enzymatic reduction of delta14-double bond of 5alpha-cholesta-8,14-dien-3beta-ol and 5alpha-cholesta-7,14-dien-3beta-ol by AY-9944. *Lipids*, **10**, 9–11.
34. Kang, M., Kim, C., Johng, T. and Paik, Y. (1995) Cholesterol biosynthesis from lanosterol: regulation and purification of rat hepatic sterol 8-isomerase. *J. Biochem.*, **117**, 819–823.
35. Shibata, M. (1993) A new potent teratogen in CD rats inducing cleft palate. *J. Toxicol. Sci.*, **18**, 171–178.
36. Honda, A., Tint, G.S., Shefer, S., Batta, A.K., Honda, M. and Salen, G. (1996) Effect of YM 9429, a potent teratogen, on cholesterol biosynthesis in cultured cells and rat liver microsomes. *Steroids*, **61**, 544–548.
37. Tozawa, R., Ishibashi, S., Osuga, J., Yagyu, H., Oka, T., Chen, Z., Ohashi, K., Perrey, S., Shionoiri, F., Yahagi, N. *et al.* (1999) Embryonic lethality and defective neural tube closure in mice lacking squalene synthase. *J. Biol. Chem.*, **274**, 30843–30848.
38. Liu, X.Y., Dangel, A.W., Kelley, R.I., Zhao, W., Denny, P., Botcherby, M., Cattanach, B., Peters, J., Hunsicker, P.R., Mallon, A.M. *et al.* (1999) The gene mutated in bare patches and striated mice encodes a novel 3beta-hydroxysteroid dehydrogenase. *Nature Genet.*, **22**, 182–187.

39. Poon, C.S., Zhou, Z. and Champagnat, J. (2000) NMDA receptor activity *in utero* averts respiratory depression and anomalous long-term depression in newborn mice. *J. Neurosci.*, **20**, RC73.
40. Kutsuwada, T., Sakimura, K., Manabe, T., Takayama, C., Katakura, N., Kushiya, E., Natsume, R., Watanabe, M., Inoue, Y., Tagi, T. *et al.* (1996) Impairment of suckling response, trigeminal neuronal pattern formation, and hippocampal LTD in NMDA receptor epsilon2 subunit mutant mice. *Neuron*, **16**, 333–344.
41. Forrest, D., Yuzaki, M., Soares, H.D., Ng, L., Luk, D.C., Sheng, M., Stewart, C.L., Morgan, J.I., Connor, J.A. and Curran, T. (1994) Targeted disruption of NMDA receptor 1 gene abolishes NMDA response and results in neonatal death. *Neuron*, **13**, 325–338.
42. Li, Y., Erzurumlu, R.S., Chen, C., Jhaveri, S. and Tonegawa, S. (1994) Wisker-related neuronal patterns fail to develop in the trigeminal brainstem nuclei of NMDAR1 knockout mice. *Cell*, **76**, 427–437.
43. Kew, J.N., Koester, A., Moreau, J.L., Jenck, F., Ouagazzal, A.M., Mutel, V., Richards, J.G., Trube, G., Fischer, G., Montkowski, A. *et al.* (2000) Functional consequences of reduction in NMDA receptor glycine affinity in mice carrying targeted point mutations in the glycine binding site. *J. Neurosci.*, **20**, 4037–4049.
44. Ikonomidou, C., Bittigau, P., Ishimaru, M.J., Wozniak, D.F., Koch, C., Genz, K., Price, M.T., Stefovska, V., Horster, F., Tenkova, T. *et al.* (2000) Ethanol-induced apoptotic neurodegeneration and fetal alcohol syndrome. *Science*, **287**, 1056–1060.
45. Maurice, T., Phan, V.L., Urani, A., Kamei, H., Noda, Y. and Nabeshima, T. (1999) Neuroactive neurosteroids as endogenous effectors for the sigma1 (sigma1) receptor: pharmacological evidence and therapeutic opportunities. *Jpn J. Pharmacol.*, **81**, 125–155.
46. Compagnone, N.A. and Mellon, S.H. (2000) Neurosteroids: biosynthesis and function of these novel neuromodulators. *Front. Neuroendocrinol.*, **21**, 1–56.
47. Moebius, F.F., Reiter, R.J., Hanner, M. and Glossmann, H. (1997) High affinity of sigma 1-binding sites for sterol isomerization inhibitors: evidence for a pharmacological relationship with the yeast sterol C8-C7 isomerase. *Br. J. Pharmacol.*, **121**, 1–6.
48. Li, E., Bestor, T.H. and Jaenisch, R. (1992) Targeted mutation of the DNA methyltransferase gene results in embryonic lethality. *Cell*, **69**, 915–926.